Stabilization of Passive Self-Bearing Motor Through D-axis Current Injection

1st Adrien Robert, 2nd Joachim Van Verdeghem, 3rd Bruno Dehez
Division of Mechatronic, Electrical Energy and Dynamic Systems (MEED),
Université catholique de Louvain (UCLouvain)
Louvain-La-Neuve, Belgium
{adrien.robert, joachim.vanverdeghem, bruno.dehez}@uclouvain.be

***Abstract*—Passive thrust self-bearing motor have been the subject of extensive research over the last few years, showing the possibility to reach the fully passive suspension of the rotor. However, this kind of machine becomes axially unstable above a certain rotation speed, requiring the introduction of an axial damping to be used on the full speed range. Recent researches have shown that when reluctant effects are present in such machines, it is possible to create an axial force through the D-axis current component. This open the way to introduce the required damping directly from the machine and not from an external system. This paper investigates this possibility by imposing, via vector control, a D-axis current component proportional to the axial velocity. It demonstrates the effectiveness of this approach through quasi-static analyses and dynamic simulations.**

***Index Terms*—Bearingless motor, Magnetic damping, Passive suspension**

I. Introduction

Passive thrust self-bearing motors (PTSBM) have shown the possibility of creating a fully passive levitation system that offers compactness, reliability, and a competitive price compared to the other bearingless motors. The PTSBM, based on an electrodynamic thrust bearing, allows creating axial levitation force thanks to currents induced in the stator winding when the rotor is axially shifted. These machines have been deeply investigated through modeling, optimization and prototyping [1], [2]. However, this kind of motor presents two main limitations.

The first is related to the evolution of the induced suspension force with the rotation speed, which prevents levitation at low speeds. It can be solved by changing the way the power supply is connected to the windings at low speed, so as to be able to actively control the axial position of the rotor [3], [4].

The second concerns the stability of the electrodynamic thrust bearing on which the motor is based. Indeed, [5], [6] have shown the appearance of dynamic instabilities above a certain rotation speed, preventing the use of this kind of machine on the full speed range without an external damping device. This limitation could find an elegant solution based on the results of a recent study on the impact of the reluctant effects resulting from the presence of a ferromagnetic circuit attached to the rotor [7]. Indeed, the latter shows that the axial variation of inductance coefficients gives rise to new suspension force components directly depending on the D-axis current.

In this context, this paper investigates the creation of damping thanks to this new force component to solve the stability problem of the PTSBM. To this end, Section II presents the machine structure, while its working principle and main equations are presented in Section III. The damping strategy is developed in Section IV, and investigated from a static and dynamic point of view in the case study of Section V.

This publication is supported by "La Région wallonne" as part of the funding of a FRIA grant.

II. Machine Structure

The PTSBM can be implemented in axial or radial flux topologies, as shown in Fig. 1, and creates levitation in the axial degree of freedom, the radial ones being maintained thanks to magnetic bearings. The stator of this motor is made of a three-phase winding, formed by a lower and an upper winding connected in parallel to the power supply. The rotor is made of Permanent magnets (PM) and ferromagnetic yokes surrounding the winding in order to introduce axial variation of the inductance coefficients. This kind of motor can also have magnetic saliency introducing an angular variation of these coefficients, which is not considered in this article.

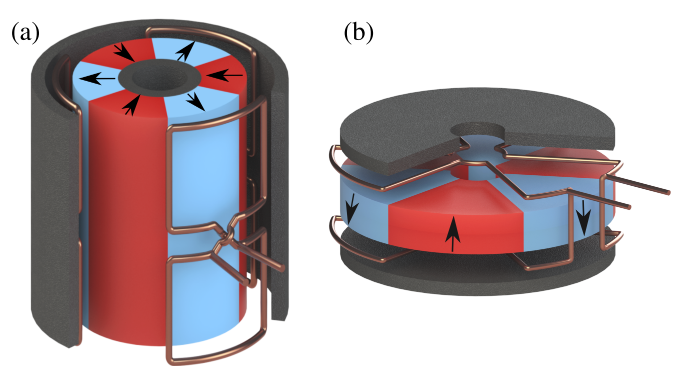

Fig. 1: Examples of PTSBM topologies with ferromagnetic materials. (a) Radial flux rotor with surface-mounted PM and ferromagnetic yokes. (b) Axial flux rotor with surface-mounted PM and ferromagnetic yokes. The ferromagnetic yokes are fixed to the rotor. Only one of the three phases is represented.

III. Working principle and modeling

This section aims to describe the working principle of the PTSBM and provides the main equations that evaluate the force and torque developed by the motor. The following developments are similar for both axial and radial flux topologies.

When the rotor is axially centered compared to the upper and lower windings, such as presented in Fig. 2(a), the flux linkages of both windings are equal, as are their back-electromotive forces (back-EMFs). In addition, the symmetry of the machine ensures that the impedance of both the upper and lower windings are identical. It results in a balanced distribution of the motor current I_M provided by the power supply between both windings, which creates a motor torque T_M but no axial force, thanks to the symmetry.

However, in the case of an axial shift of this rotor, as shown in Fig. 2(b), there is no more symmetry of the back-EMFs, which induces a current in the closed circuit formed by the connection of upper and lower windings. Moreover, due to the ferromagnetic circuit of the rotor, the inductance coefficients of both windings evolve in the opposite direction, which unbalances the impedance and then the distribution of the current provided by the source. The current imbalance and the induced current compose the suspension current I_S, a differential current that flows in opposite direction in the upper and the lower winding. This flowing direction produces a net axial force F_z opposed to the axial shift, but also a parasitic torque T_P which is superposed and generally opposed to the motor torque.

Firstly, let us describe the total suspension force created by the motor in quasi-static conditions with the equation (1), presented on the bottom of the page. The latter introduces the axial position of the rotor, z, the rotation speed, ω, the synchronous suspension inductance (defined in [7]) and its gradient, $L_{S,c}$ and $L_{z,c}$, the D and Q-axis motor currents, $I_{M,d}$ and $I_{M,q}$, and the axial gradient of the flux linkages, $K_{\theta,z}$. Equation (1) shows that the force increases with the rotation speed up to reach an asymptotic value. This evolution depends on the electrical pole ω_e of the machine, defined as:

$$\omega_e = \frac{R}{pL_{S,c}} \tag{2}$$

with the number of pole pair of the motor, p, and the phase resistance of an upper/lower winding, R. As the force depends linearly on the axial shift of the rotor, it is possible to defined an asymptotic stiffness k_{tot}^{∞}, which characterizes the suspension capability of the motor, regardless of axial shift and rotation speed. Equation (1) shows that this total asymptotic stiffness has three components: an electrodynamic stiffness k_{ed}^{∞}, created by the axial variation of the flux linkages, a reluctant stiffness k_{rel}^{∞}, which depends on the axial variations of the inductance coefficient, and a cross stiffness k_{cross}^{∞}, which appears when both phenomena coexist.

Secondly, the combination of the motor and parasitic torques provides the total torque developed by the motor under quasi-static conditions:

$$\begin{aligned} T_{tot} = & \sqrt{\frac{3}{2}} pK_\theta \cdot I_{M,q} \\ & - z^2 \frac{\omega^2}{\omega^2+\omega_e^2} \cdot \sqrt{\frac{3}{2}} pK_{\theta,z} \cdot \frac{L_{z,c}}{L_{S,c}} \cdot I_{M,q} \\ & - z^2 \frac{\omega \cdot \omega_e}{\omega^2+\omega_e^2} \left(\frac{3pK_{\theta,z}^2}{L_{S,c}} + \sqrt{\frac{3}{2}} pK_{\theta,z} \cdot \frac{L_{z,c}}{L_{S,c}} \cdot I_{M,d} \right) \end{aligned} \tag{3}$$

with the amplitude of the flux linkages, K_θ.

Finally, from the stability point of view, the electrical pole ω_e also represents the rotation speed threshold above which the machine becomes axially unstable. According to [6], it is possible to define $C_{z,min}$, the minimal damping value required to ensure the stability of the machine on the full speed range:

$$C_{z,min} = \frac{k_{tot}^{\infty} \cdot L_{S,c}}{8R} \tag{4}$$

To date, it was considered that this damping could only be provided by the action of an external system.

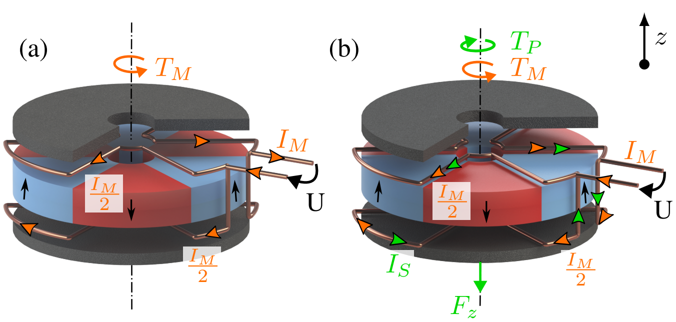

Fig. 2: Working principle of the passive thrust self-bearing machine with an axial flux surface mounted rotor and ferromagnetic yokes. (a) Centered position. (b) Off-center position.

IV. Damping strategy

This section presents the damping strategy investigated in this paper and its corresponding stability criteria. The control scheme implementing this strategy is also presented.

$$F_z = -z \cdot \frac{\omega^2}{\omega^2+\omega_e^2} \cdot k_{tot}^{\infty} = -z \cdot \frac{\omega^2}{\omega^2+\omega_e^2} \cdot \left(\underbrace{\frac{3K_{\theta,z}^2}{L_{S,c}}}_{k_{ed}^{\infty}} + \underbrace{\frac{L_{z,c}^2}{2L_{S,c}} \cdot \left(I_{M,d}^2 + I_{M,q}^2\right)}_{k_{rel}^{\infty}} + \underbrace{\sqrt{6} \cdot K_{\theta,z} \cdot \frac{L_{z,c}}{L_{S,c}} \cdot I_{M,d}}_{k_{cross}^{\infty}} \right) \tag{1}$$

A. Damping strategy and stability criteria

Equation (1) shows that the cross force term, related to the cross stiffness k^{∞}_{cross}, which appears when axial variation of both the inductance and the flux coexists, are linearly dependent on the D-axis motor current $I_{M,d}$. To produce damping, let us consider this current proportional to the axial speed of the motor $\dot{z}$ such that:

$$I_{M,d} = K_p \cdot \dot{z} \cdot sign(z) \tag{5}$$

with a proportional gain K_p. The factor $sign(z)$ is required to ensure a damping force opposed to the axial speed, since the equation (1) is already proportional to the axial position. Injecting (5) in (1) allows separating the total force developed by the motor in two terms:

$$\begin{aligned} F = & - z \underbrace{\frac{\omega^2}{\omega^2+\omega_e^2} \cdot \left[\frac{3K_{\theta,z}^2}{L_{S,c}} + \frac{L_{z,c}^2}{2L_{S,c}} \cdot I_{M,q}^2 \right]}_{k_{tot}} \\ & - \dot{z} \cdot \underbrace{z \cdot sign(z) \cdot \frac{\omega^2}{\omega^2+\omega_e^2} \cdot \left[\sqrt{6} \cdot K_{\theta,z} \cdot \frac{L_{z,c}}{L_{S,c}} \cdot K_p \right]}_{C_{z,I_{M,d}}} \end{aligned} \tag{6}$$

The term proportional to $\dot{z}^2$ is neglected by considering small axial speed $\dot{z}$. This assumption will be verified int the case study in Section V. Equation (6) makes appear two force components, a spring force, proportional to the axial shift z, and a damping force, proportional to the axial speed $\dot{z}$, the latter being characterized through a damping coefficient:

$$C_{z,I_{Md}} = |z| \cdot \frac{\omega^2}{\omega_e^2 + \omega^2} \cdot \sqrt{6} \cdot K_{\theta,z} \cdot \frac{L_{d,z}}{L_{S,d}} \cdot K_p \tag{7}$$

This expression depends on the rotation speed and the axial position. Considering a steady state with a constant external force F_e applied to the rotor, e.g., the weight, allows to fix the mean axial position:

$$|z| = \frac{|F_e|}{k_{tot}} = \frac{|F_e|}{\frac{\omega^2}{\omega_e^2+\omega^2} \cdot k^{\infty}_{tot}} \tag{8}$$

Injecting the latter in (7) suppresses the dependence of the damping coefficient on the rotation speed and the axial position, yielding:

$$C_{z,I_{Md}} = \frac{|F_e|}{k^{\infty}_{tot}} \cdot \sqrt{6} \cdot K_{\theta,z} \cdot \frac{L_{d,z}}{L_{S,d}} \cdot K_p \tag{9}$$

Finally, on the basis of (4), it is then possible to determine the minimum value of K_p guaranteeing stable machine behavior around the working point under consideration, over the entire speed range:

$$K_p = \frac{(k^{\infty}_{tot} \cdot L_{S,c})^2}{8\sqrt{6} \cdot RK_{\theta,z}L_{z,c} \cdot |F_e|} \tag{10}$$

B. Control scheme

The motor control scheme able to implement this damping strategy, which will be named I_d-damping, is a classical two-level vector control, with decoupling between the D and Q-axis motor current and back-emf compensation. However, conversely to the classical PTSBM, where the D-axis current reference is set to zero, the latter is controlled to be proportional to the axial speed $\dot{z}$ of the rotor, according to (5) and as represented in Fig. 3. The latter also introduces $L_{M,c}$, the synchronous motor inductance coefficient defined in [7].

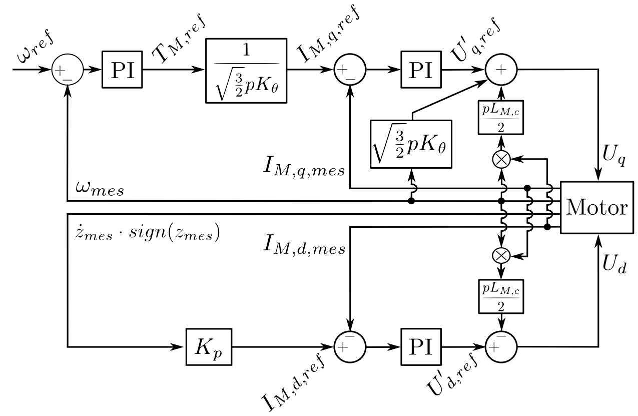

Fig. 3: Speed control schematic used to control the axial and rotation speed of the PTSBM. Decoupling between d and q axis current is applied, such as a back-EMF compensation.

V. Case Study

This section aims to validate the proposed damping method thanks to a case study simulated with Matlab Simulink, based on the electromechanical model introduced in [7], which describes the rotor dynamics of a PTSBM. The motor under study and its dimensions are described in Fig. 4 and Table I. Section V-A and V-B respectively study the stability and the dynamic behavior of the chosen machine.

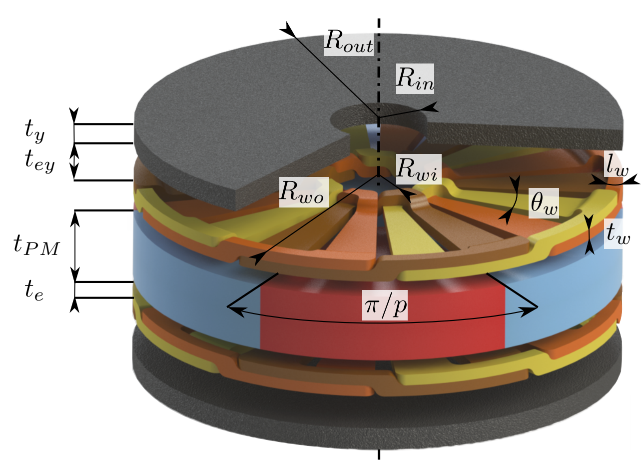

Fig. 4: Geometrical parameters of the motor under study with the three phases represented

TABLE I: Geometric, electric and magnetic parameters of the chosen case study

Parameter	Symbol	Unit	Value	Parameter	Symbol	Unit	Value
			Geometrical parameters				
Number of pole pairs	p	-	4	Volume of PM	V_{PM}	cm^3	32
Mass	m	kg	0.42	Polar moment of inertia	J	$kg \cdot m^2/rad$	$8.4 \cdot 10^{-4}$
Rotor outer radius	R_{out}	mm	60	Rotor inner radius	R_{in}	mm	20
Winding outer radius	R_{wo}	mm	65	Winding inner radius	R_{wi}	mm	25
Air gap between PM and winding	t_e	mm	0.75	Permanent magnet thickness	t_{PM}	mm	10
Air gap between yoke and winding	t_{ey}	mm	0.75	Iron yoke thickness	t_y	mm	3
Angular opening coefficient of windings	c_o	-	0.9	Number of phase	N	-	3
Winding thickness	t_w	mm	7.5	Number of spire per phase	n_s	-	12
Winding angular opening	θ_w	rad	$\frac{c_o \cdot \pi}{N \cdot p} = 0.23$	Winding width	l_w	mm	$\frac{R_{wi} \cdot \theta_w}{1-\theta_w} = 7.7$
			Electrical and magnetic parameters				
Remanent flux of the ferrites	Br	T	0.6	Upper phase resistance	R	$m\Omega$	70
Flux amplitude	K_θ	mWb	7.4	Gradient of the flux amplitude	$K_{\theta,z}$	Wb/m	0.508
Motor inductance	L_M	μH	34	Suspension inductance	$L_{S,c}$	μH	22.4
Axial gradiant of inductances	$L_{z,c}$	mH/m	-1.81				

A. Stability analysis

The electromechanical model of the PTSBM, presented in [7], can be expressed under its canonical state space form:

$$\dot{\mathbf{x}} = \mathrm{f}(\mathbf{x}, \mathbf{u}, \mathbf{v}) \tag{11}$$

with $\mathbf{x}$, $\mathbf{u}$, and $\mathbf{v}$, respectively the state, input and disturbance vectors, defined as:

$$\mathbf{x} = \begin{bmatrix} I_{M,d} & I_{M,q} & I_{S,d} & I_{S,q} & z & \dot{z} & \omega \end{bmatrix}^{\mathrm{T}} \tag{12}$$

$$\mathbf{u} = \begin{bmatrix} U_d & U_q \end{bmatrix}^{\mathrm{T}} \quad \mathbf{v} = \begin{bmatrix} F_e & T_e \end{bmatrix}^{\mathrm{T}} \tag{13}$$

where $I_{S,d}$ and $I_{S,q}$ are the D and Q-axis suspension currents, U_d and U_q, the input voltages, and F_e and T_e, the external force and torque applied on the rotor.

To investigate the impact of the D-axis damping on the stability, the eigenvalues of the system can be computed. To this end, the system of equation (11) is linearized around an equilibrium point defined by a constant rotation speed, an external torque T_e of $0.4[Nm]$, and an external force F_e of $4.1[N]$, equal to the weight of the rotor. The latter leads, using (10) to ensure the stability, to a value of $K_P = -113.5[sA/m]$ whose negative sign comes from the sign of the axial inductance gradient $L_{z,c}$. Solving (11) under these conditions allows to determine the equilibrium point, defined by the vectors $\mathbf{x}^*$, $\mathbf{u}^*$ and $\mathbf{v}^*$, around which the system can be linearized thanks to a first-order Taylor approximation:

$$\dot{\tilde{\mathbf{x}}} = \mathbf{A} \cdot \tilde{\mathbf{x}} + \mathbf{B} \cdot \tilde{\mathbf{u}} + \mathbf{C} \cdot \tilde{\mathbf{v}} \tag{14}$$

with the vectors $\tilde{\mathbf{x}} = (\mathbf{x} - \mathbf{x}^*)$, $\tilde{\mathbf{u}} = (\mathbf{u} - \mathbf{u}^*)$, and $\tilde{\mathbf{v}} = (\mathbf{v} - \mathbf{v}^*)$. This linearized system is then injected in the control scheme of Fig. 3, and the eigenvalues of this complete equivalent system are computed for different K_p values.

Fig. 5(a) shows the evolution of these eigenvalues with the rotation speed while Fig. 5(b) zooms in on the mechanical eigenvalues. The latter highlights, first, the low rotation speed instabilities that ensue from the coupling between axial and

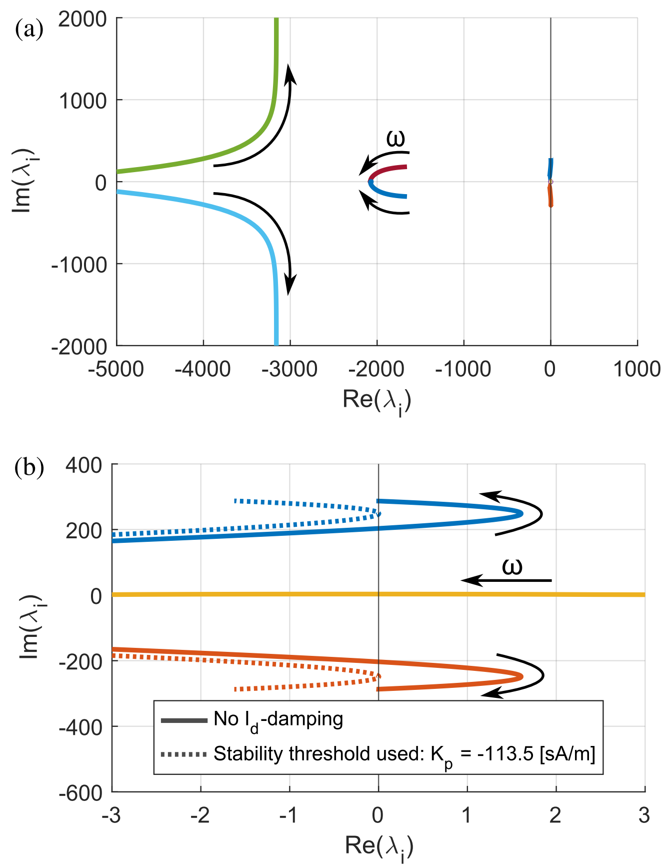

Fig. 5: (a) Evolution of the seven eigenvalues λ_i of the machine with the rotation speed, for $\omega \in [100 - 100\,000][rad/s]$. (b) Zoom on the relevant eigenvalues. The latter are computed with and without I_d-damping to observe the sliding of the eigenvalues related to the axial dynamics, the most upper and lower curves of the second figure, in the stability zone. The other eigenvalues, much less impacted by the I_d-damping, are not represented for the second case.

rotation dynamics, as discussed in [6]. However, they appear for a speed range for which the induced force is not sufficient to create the levitation. These first instabilities are therefore not a cause of concern. However, the blue upper and red lower curves in Fig. 5(b), linked to the axial dynamics, show the arising of the instability when the rotation speed increases.

As explained in [5], the eigenvalues related to axial dynamics reach their largest real part, i.e. the most critical value in terms of stability, when the rotation speed equals $\omega = \sqrt{3}\omega_e$. It also means that, for this rotation speed, using I_d-damping designed with the stability threshold gain (10) should align the eigenvalues with the imaginary axis. It is verified by the two doted lines in Fig. 5(b), which represent the evolution of these eigenvalues in this situation. Both curves have consistently been shifted towards the left until the rightmost eigenvalue nearly aligns with the imaginary axis. Interestingly, the value obtained from equation (10) doesn't perfectly match the right limit alignment with the vertical axis. This discrepancy can be attributed to the simplification made when neglecting quadratic axial speed terms in equation (6). However, it shows that the stability criteria for the proportional gain proposed in (10) suits well to ensure the axial stability in the whole speed range.

B. Dynamic behavior

This section evaluates the dynamic behavior of the PTSBM on which is applied the strategy of I_d-damping. Fig. 6 depicts the evolution of the axial position and the D-axis current when, in addition to the weight, an external disturbance force of $1[N]$ is applied on the rotor during $10[ms]$. The test is performed for a rotation speed of $\omega = \sqrt{3}\omega_e$. As explained previously, this rotation speed maximizes the real parts of the eigenvalues related to axial dynamics, and is therefore the most critical situation in terms of stability. This instability appearing without damping is illustrated in Fig. 6(a). The latter also shows the same test when activating the proposed I_d-damping strategy, designed with the stability threshold gain (10). As shown in the previous section, it aligns the eigenvalues with the imaginary axis, which leads to a marginally stable axial dynamics. Finally in case of higher gain, the PTSBM becomes stable for all rotation speeds. Fig. 6(b) shows the amplitude of the D-axis current reached depending on the value of the gain used. It shows that a gain three times higher than the stability threshold provides a maximum peak current of $6[A]$. Since the constant Q-axis current providing the $0.4[Nm]$ of motor torque is equal to $10.2[A]$, this value is acceptable.

Fig. 7 studies the impact of the rotation speed on the axial dynamics, in a test similar to the previous, and with a constant value of K_p $(-113.5[sA/m])$. The rotation speed $\omega = \sqrt{3}\omega_e$, at which the rotor shows a marginally stable dynamics with this value of gain, taken as reference. The figure shows that the damping strategy manages to stabilize the rotor for both speeds higher and lower than the reference one, which is consistent with Fig. 5(b) since the eigenvalues of rotation speeds higher and lower than $\sqrt{3}\omega_e$ lead to more stable dynamics. Finally, as the axial force rises with the rotation speed, the higher this speed, the lower the mean axial position.

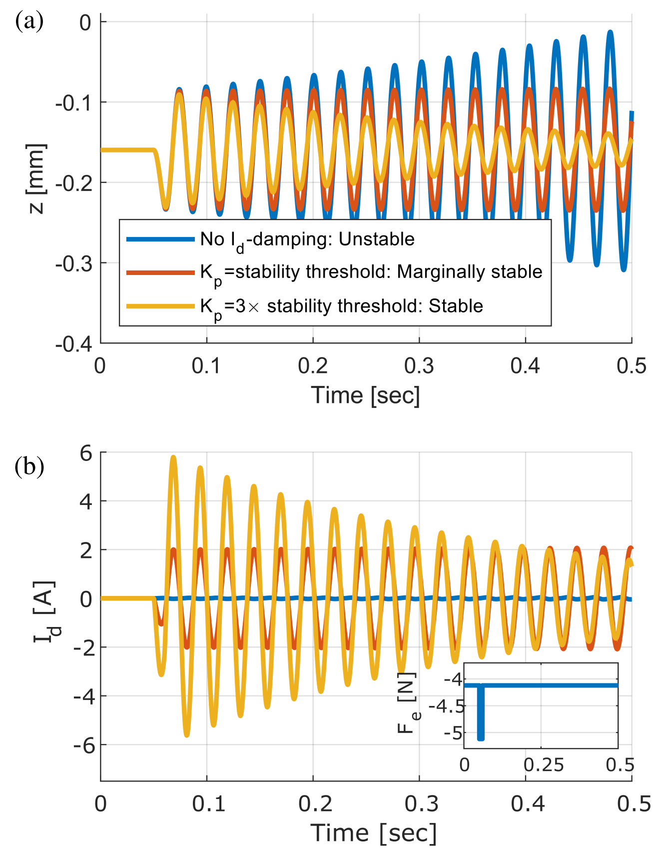

Fig. 6: *Impact of the gain K_p* - Application of a disturbing step force of $-1[N]$ on the rotor at $t \in [0.05 - 0.06][sec]$, for $\omega = \sqrt{3}\omega_e = 10\ 146[rpm]$ and with a driving torque of $0.4[Nm]$. An external force, corresponding to the weight, is also applied on the rotor and different values of gain are tested for the control of the D-axis. (a) Axial position. (b) D-axis current.

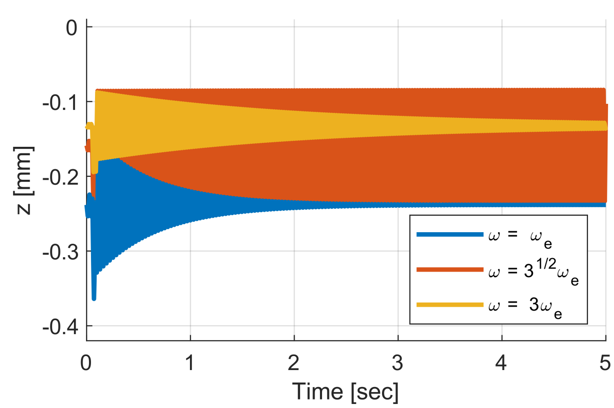

Fig. 7: *Impact of the rotation speed ω* - Axial position for similar test condition than the previous figure, but for a constant value of K_p $(-113.5[sA/m])$ and different rotation speeds

The impact of the mean external force applied to the rotor is studied in Fig. 8 to conclude the analysis. Once again, the test is similar to what was done for Fig. 6 and 7, but for a constant rotation speed of $\omega = \sqrt{3}\omega_e$ and a constant value of K_p ($-113.5[sA/m]$). However, kepping this gain constant, the amplitude of the constant external force applied to the rotor varies from zero to twice the weight. The upper blue curve of the figure corresponds to a zero constant external force, and then an axially centered rotor, which occurs when the weight is fully compensated by an external device. In this situation, reaching the stability would require an infinite value of K_p, as shown by equation (10). However, the axial oscillation amplitude does not exponentially increase but reaches a limit cycle. Indeed, even if the I_d-damping strategy does not ensure the stability in centered position since no damping force occurs in $z = 0$, the injection of D-axis current still creates some force opposed to the axial speed when the rotor is off-centered during the oscillation, and therefore prevents instability. An asymmetry of the d-axis current, caused by the non-linear $sign(z)$-factor occurring in the control, is also visible in Fig. 8(b). On the other hand, if the constant external force is higher than the force corresponding to the gravity, e.g. if the axial load has been incorrectly estimated, the I_d-damping manages to stabilize the rotor. It is explained by (10), as an increase of the constant external force leads to a diminution of the minimal required gain value to ensure the stability.

a) Assumption validation

Let us finally verify the assumption made to obtain (6), which neglects the force proportional to $\dot{z}^2$ in case of D-axis current proportional to $\dot{z}$. To that end, the ratio between this force and the force linearly proportional to the speed, from (6), is computed for the maximal axial speed, $\dot{z}_{max} = 0.02[m/s]$ obtained in the simulation:

$$\frac{F \propto \dot{z}^2}{F \propto \dot{z}} = \frac{L_{z,c} \cdot K_p \cdot \dot{z}_{max}}{2\sqrt{6} \cdot K_{\theta,z}} = 1.6 \cdot 10^{-3} \quad (15)$$

It shows that the assumption that neglects the term proportional to $\dot{z}^2$ is valid.

VI. Conclusion

This paper introduces, for a passive thrust self-bearing machine subjected to axial reluctance effects, a new damping strategy based on the injection of D-axis current, the amplitude of the latter being proportional to the axial speed of the rotor. It also proposes a design method for the gain of the controller, based on a stability criteria, which ensures the stability of the machine on the whole speed range around a working point. This design method has been validated, first, with the analysis of the linearized system eigenvalues and, secondly, through numerical simulation in dynamic conditions.

Future works will aim to validate experimentally this new damping strategy, but also investigate the possibility to estimate the axial speed and position of the rotor used to create the damping, through sensorless method.

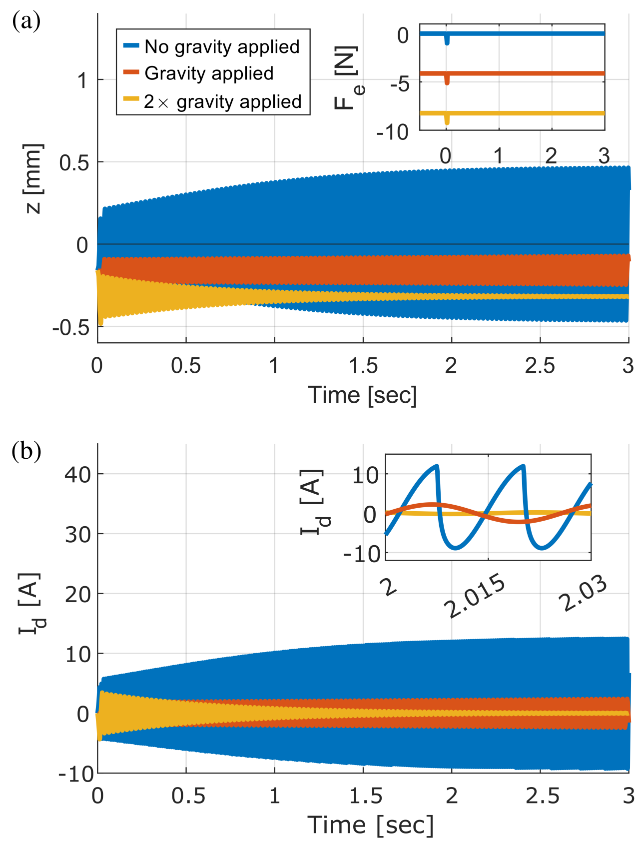

Fig. 8: *Impact of the constant external force* - similar test condition than the two previous figures, but for a constant value of K_p ($-113.5[sA/m]$) and $\omega = \sqrt{3}{\cdot}\omega_e = 10\ 146[rpm]$. The amplitude of the constant external force varies from zero to twice the weight of the rotor. (a) Axial position. (b) D-axis current.

References

[1] J. Van Verdeghem and B. Dehez, "Fully Passively Levitated Self-Bearing Machine Implemented Within a Reaction Wheel," *IEEE Transactions on Industry Applications*, vol. 57, no. 6, pp. 5782–5795, Nov. 2021.

[2] G. C. Rubio, V. C. Hothur Komal, Y. Fujii, and A. Chiba, "Experimental Verification of Passive Axial Electrodynamic Suspension in a Bearingless Motor," *IEEE Open Journal of Industry Applications*, pp. 1–12, 2023.

[3] J. Van Verdeghem, E. L. Severson, and B. Dehez, "Hybrid Active–Passive Actuation Approach of Passively Levitated Thrust Self-Bearing Machines," *IEEE Transactions on Industry Applications*, vol. 57, no. 6, pp. 7035–7045, Nov. 2021.

[4] J. V. Verdeghem and B. Dehez, "Observer-based Self-Sensing Techniques for Hybrid Active-Passive Self-Bearing Machines," in *The 18th International Symposium on Magnetic Bearings*, Lyon, France, Jul. 2023.

[5] J. Van Verdeghem, V. Kluyskens, and B. Dehez, "Stability and Performance Analysis of Electrodynamic Thrust Bearings," *Actuators*, vol. 8, no. 1, p. 11, Mar. 2019.

[6] J. Van Verdeghem, M. Lefebvre, V. Kluyskens, and B. Dehez, "Dynamical Modeling of Passively Levitated Electrodynamic Thrust Self-Bearing Machines," *IEEE Transactions on Industry Applications*, vol. 55, no. 2, pp. 1447–1460, Mar. 2019.

[7] J. Van Verdeghem, A. Robert, S. Herrman, and B. Dehez, "Impact of Ferromagnetic Yokes on Axial Flux Passively Levitated Self-Bearing Machines," in *2022 25th International Conference on Electrical Machines and Systems (ICEMS)*, Nov. 2022, pp. 1–6.